The Canadian Mineralogist
Vol. 59, pp. 9-30 (2021)
DOI: 10.3749/canmin.2000061

STRUCTURE TOPOLOGY AND GRAPHICAL REPRESENTATION OF DECORATED AND UNDECORATED CHAINS OF EDGE-SHARING OCTAHEDRA

AARON J. LUSSIER[§]

Canadian Museum of Nature, P.O. Box 3443, Station D, Ottawa, Ontario, K1P 6P4

FRANK C. HAWTHORNE

Department of Geological Sciences, University of Manitoba, 125 Dysart Road, Winnipeg, Manitoba, R3T 2N2, Canada

ABSTRACT

Infinite chains of edge-sharing octahedra occur as fundamental building blocks (FBBs) in the structures of several hundred mineral species. Such chains consist of a backbone of octahedra to which decorating polyhedra may be attached. The general, stoichiometric formula of such chains may be written as $^{c}[M_A T_x \Phi_z]$ where M is any octahedrally coordinated cation, T is any cation coordinated by a decoration polyhedron (regardless of coordination geometry), Φ is any possible ligand [O^{2-}, $(OH)^-$, (H_2O), Cl^-, or F^-], and c indicates the configuration of backbone octahedra. In the minerals in which they occur, these types of chains will commonly (though not exclusively) form part of the structural unit (*i.e.*, the strongly bonded part) of a mineral. Hence, investigating the topology, configuration, and arrangement of such chains may yield fundamental insights into the stability of minerals in which they occur. A discussion of the topological variability of chains is presented here, along with the formulae necessary for their characterization. It is shown that many aspects of chain topology can be efficiently communicated by a pair of values with the form ([x], [*Bopqrst*]), where [x] summarizes the symmetry operations necessary to characterize the configuration of backbone octahedra, *B* indicates the length of the topological repeat, and *o* through *t* indicate the number of individual decorations (related to *B*). A methodology for developing finite graphical representations for infinite chains is presented in detail, showing that for any given chain, a single, irreducible finite graph exists that contains all topological information. Such a graph, however, can correspond to multiple chain topologies, highlighting the importance of geometrical isomerism. The utility of the graphical approach in facilitating the development of a hierarchy of chains and chain-bearing structures is also discussed.

Keywords: chains of edge-sharing octahedra, [$M\Phi_4$] chains, chain backbone, chain decoration, graphical representation, graphical isomer, geometrical isomer, structural unit.

INTRODUCTION

Infinite chains of octahedra are common topological features in the structures of oxysalt compounds. They can be considered as Fundamental Building Blocks (FBBs) occurring in at least several hundred mineral species and synthetic compounds. Three fundamental types of chains can be distinguished on the basis of whether constituent octahedra are connected by vertex-, edge-, or face-sharing, corresponding to the general stoichiometries $^{\infty}[M\Phi_5]$, $^{\infty}[M\Phi_4]$, and $^{\infty}[M\Phi_3]$, respectively [where M = any cation in octahedral coordination and Φ = an unspecified ligand, typically O^{2-}, $(OH)^-$, (H_2O), F^-, or Cl^-].

In a subsequent series of papers, we will focus on the topology, frequency, and occurrence of the edge-sharing chains in minerals. These chains are commonly observed with decoration polyhedra (*e.g.*, tetrahedra, trigonal planar groups) attached. Through the variation in configuration of backbone octahedra, chain repeat distance, and connectivity (and abundance) of decoration polyhedra, a very large number of possible topologies may be derived. This high degree of complexity makes the characterization and discussion of chains a non-trivial task; here, a systematic

---

[§] *Corresponding author e-mail address*: alussier@nature.ca method for presenting this information, both mathematically and graphically, is rigorously derived and presented. This methodology will be essential to developing and elucidating the geometric constraints of such chains, the graphical enumeration of possible topologies, and the hierarchical ordering of structures in which chains are essential components of the structural unit.

PREVIOUS WORK

In a pioneering paper, Moore (1970) considered the structure hierarchy of chains of octahedra and tetrahedra of the form [$M\Phi_5$]. He derived all possible [$M\Phi_5$] chains with a repeat distance of ~7.2 Å (corresponding to two octahedra in the repeat unit) and showed that numerous minerals are based on these chains. Moore & Araki (1974, 1977) followed with detailed studies of various combinatorial polymorphs, and there has been subsequent work done on these [$M\Phi_5$] chain structures (*e.g.*, Hawthorne 1983, Burns & Hawthorne 1995) that has focused on the linkage of such chains into sheets and frameworks. Surprisingly, there has been little analogous work on chains of edge-sharing octahedra in minerals. There have been general surveys done as part of the development of structure hierarchies involving oxyanions that decorate such chains (*e.g.*, Hawthorne 1985, 1986, 1990, 1998, Hawthorne *et al*. 2000, Huminicki & Hawthorne 2002) or detailed crystal chemistry on specific types of chains (*e.g.*, Sokolova & Hawthorne 2004, Fleck *et al*. 2002, Fleck & Kolitsch 2003, Kolitsch & Fleck 2005). However, there has been no general work on their topology.

CHAINS OF EDGE-SHARING OCTAHEDRA: TERMINOLOGY

Chain: A structural unit of $(M\Phi_6)^{n-}$ octahedra that link infinitely in a single direction and that can be broken by eliminating a single $(M\Phi_6)^{n-}$ octahedron (Figs. 1a, b).

Ribbon: A structural unit of $(M\Phi_6)^{n-}$ octahedra that link infinitely in a single direction and that cannot be broken by eliminating any single $(M\Phi_6)^{n-}$ octahedron (Fig. 1c). This work focuses on the characterization of chains; ribbons will be addressed in a future publication.

Backbone: Backbone octahedra are essential to the existence of a chain; each backbone octahedron shares edges with *at least* two other backbone octahedra.

Decoration: Additional polyhedra, denoted by $(T\Phi_m)^{n-}$, that decorate (link to) the backbone octahedra and that are not essential for chain continuity. The value of m corresponds to the coordination number of the T cation, hence values of 3, 4, 5, and 6 correspond to planar triangles, tetrahedra, pentahedral–hexahedral polyhedra, and octahedra, respectively. Where a stereoactive lone-pair of electrons emanates from the central cation, it is represented by E, such as $T\Phi_3E$. An anion belonging to a decoration polyhedron that does not link to backbone octahedra is referred to as an ω-anion (Fig. 1b).

Crystallographic repeat unit: The minimal geometrical arrangement of backbone octahedra (and element-sharing decorations) required to generate the chain *via* translation.

A list of all variables used throughout this text, with definitions, is given in Table 1.

CONFIGURATION OF BACKBONE OCTAHEDRA IN EDGE-SHARING CHAINS

In an infinite chain of edge-sharing octahedra, each backbone octahedron shares (at least) two of its twelve edges with two different octahedra. Backbone configurations can be readily distinguished based on the symmetry operations that relate the shared edges on any given backbone octahedron. The symmetry of a holosymmetric octahedron (point group $4/m\bar{3}2/m$), is as follows: 16 three-fold axes (eight proper, eight improper), 15 four-fold axes (nine proper, six improper), six two-fold axis, nine mirror planes, and an inversion center. As successive octahedra are added to form a complete chain, each set of shared edges on a particular octahedron can be related by an appropriate symmetry operation.

All possible sets of shared edges in non-*cis* chains (see discussion below) associated with a single octahedron are related by one of the [2]-fold axes of the octahedron. In Figure 2a, each diad is illustrated using a separate color: the solid-color dots indicate the location where the axis enters/exits the octahedron, and similar lines (dashing/shading) show those edges related by the [2]-fold symmetry operation. The axes are numbered, increasing clockwise about the [3]-fold axis of the octahedron.

Figure 2b shows how an arbitrary non-*cis* chain can be constructed through a defined sequence of [2]-fold operators. For instance, using the orientation of the octahedron in Figure 2a as a reference, the chain results from the sequence given by the row matrix, [x], [1 6 1 3 4 3]. As they occur in the chain, however, the [2]-fold axes, labeled 6 and 4 in Figure 2a, are equivalent to the inversion operation, *i*, about the center of the octahedron and thus we will simplify to [x] = [1 *i* 1 3 *i* 3].

The absolute orientation of the [2]-fold axis is arbitrary, providing they are named sequentially about an octahedral [3]-fold axis, and hence it is the relative difference between these that defines the backbone

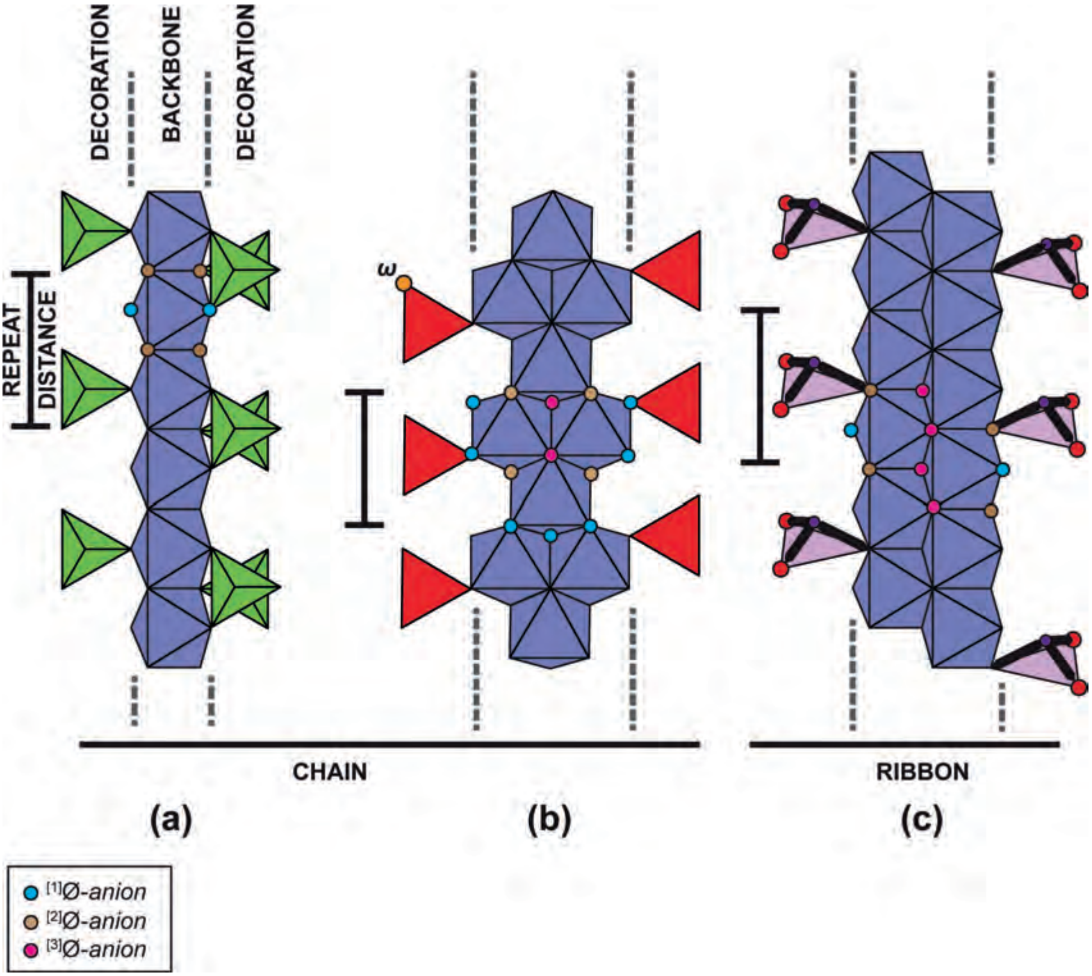

FIG. 1. Basic components of (a–b) infinite chains and (c) ribbons composed of edge-sharing octahedra: backbone structure and decoration polyhedra of differing coordination. Anion positions are labeled as discussed in the text.

configuration. Labeling the first, arbitrarily-chosen, [2]-fold operator as *D* gives [x] = [*D i D D*+2 *i D*+2].

Common chain backbones

If the repeat distance is considered variable, an infinite number of possible chain backbone configurations are possible. However, an examination of chain-bearing structures in the literature suggests that four basic types of backbone configurations occur with significant frequency in minerals. These are illustrated in Figure 3. As these are common, they can be more easily referred to by the following names in subsequent discussion: *trans*, *lox*, *mik*, and *cis* (defined below).

In a *trans* chain [x] = [*i*] (Fig. 3a), both linking edges on any octahedron are related by inversion through the octahedron center. The resulting undecorated chain is (ideally) symmetric about three orthogonal mirror planes and three orthogonal [2]-fold axes. In a *lox* (Greek: *loxótita*, skew) chain, linking edges are related by one rotation around the [2]-fold axis of the central octahedron. There are two *lox* backbone configurations, referred to here as *lox,* [x] = [*D*] (Fig. 3b) and *lox*-I, [x] = [*D D D*+2 *D*+2] (Fig. 3c). In a *mik* (Greek: *miktós*, mixed) chain, any combination of *trans* and *lox* linkages may occur. An example of a common *mik* chain (occurring in minerals such as borax and mirabilite) corresponding

TABLE 1. LIST AND DEFINITIONS OF VARIABLES AND FUNCTIONS USED THROUGHOUT THE CURRENT WORK

M	Any octahedrally coordinated cation in the backbone of an infinite chain.
T	Any m-coordinated cation in a decoration polyhedron, ($T\Phi_{\mathrm{m}}$), attached to a chain backbone.
Φ	Any possible ligand [O^{2-}, $(OH)^{-}$, (H_2O), Cl^{-}, or F^{-}].
A, X, z	In the general formulae written in stoichiometric ${}^{c}[\ M_A T_X \Phi_z\ ]$ (Eq. 1) or matrix ${}^{c}[\ A\ X\ z\ ]_{\infty}$ (Eq. 3) form, variables A, X, and z represent the stoichiometric quantity of M-octahedra, T-decorations, and Φ-ligands. Variable A also corresponds to the number of octahedra in the repeat unit of the chain.
h, i, j, k	Variables indicating the stoichiometric content of decoration polyhedra with distinct coordination number, as in $(T\Phi_6)_i\ (T\Phi_5)_j\ (T\Phi_4)_k\ (T\Phi_3E)_l\ (T\Phi_3)_m$, where $i + j + k + l = X$.
[$Bopqrst$]	In the topological (graphical) formulae written in stoichiometric ([x], [M_B (${}^{[4]}\Delta[v,3]_{\mathrm{n}}\ {}^{[2+3+2]}\Delta[e,2]_o\ {}^{[2+3]}\Delta[v,3]_p\ {}^{[2+2]}\Delta[v,2]_q\ {}^{[3]}\Delta[v,2]_r\ {}^{[2]}\Delta[v,1]_s$)]) or matrix ([x], [B o p q r s t]) form, B represents the number of backbone vertices, where as o through t represents the number of vertices of each color, corresponding to different decoration polyhedra, with different values of ${}^{\Sigma a}\Delta[s,N]$.
[x]	Denotes a row matrix of integers indicating the sequence of octahedral [2]-fold axes that results in a specific linking configuration of backbone octahedra.
B'	The number of backbone (purple) vertices required in the topological repeat graph.
${}^{[Cn]}\Phi$	Denotes the coordination number, Cn, of the anion(s) linking decoration polyhedra to backbone octahedra.
${}^{\Sigma a}\Delta[s,N]$, ${}^{\Sigma a}\Omega[s,N]$	Denotes the overall configuration of decoration polyhedra (Δ) or an added backbone octahedra (Ω), as defined by the coordination number, a, of each linking anion. In square brackets, s, indicates the polyhedral element shared between decoration and backbone octahedra (v, vertex; e, edge; f, face). N indicates the number of individual backbone octahedra to which a given decoration is linked.
$V(G)$	The vertex-set of a graph.
$E(G)$	The edge-set of a graph.
$\sum K_i$	[$= V(G)$], represents the total vertex set, broken down into individual, K-colored components.

to $[x] = [\ D\ D\ i\ ]$ is given in Figure 3d. The arbitrary chain illustrated in Figure 2b also corresponds to a *mik* chain. In a *cis* chain, certain backbone octahedra have more than two shared edges, and these edges share a common vertex. An infinite number of mik configurations are possible, and the stoichiometry of the chain backbone varies accordingly. Figure 3e illustrates an example, although many configurations of *cis* chain are possible.

The basic connectivity of each chain backbone is also shown graphically; each purple vertex denotes a backbone octahedron and each edge denotes a shared octahedron vertex. Edges shared between octahedra are shown as pairs of edges in the graph. Backbones with *trans*, *lox*, and *mik* conformations have the same graphical representation, whereas those with *cis* conformations do not.

Above, we noted that non-*cis* chains can be constructed *via* a sequence of [2]-fold rotation operators or a sequence of [2]-fold rotation operators and inversion centers. However, it is preferable to use i when possible. The reason for this can be seen when comparing the *trans* and *lox* chains in Figures 3a and 3b. Relative to a [2]-fold rotation axis, both chains result from the repetition of one [2]-fold axis orientation, hence both would correspond to $[x] = [\ D\ ]$, which is clearly not useful. However, referring to sequences with inversion operators results in the matrices $[x] = [\ i\ ]$ and $[x] = [\ D\ ]$, respectively, differentiating the two backbone configurations.

Backbone anion notation

Constituent anions of backbone chains occur in three types of coordinations, characterized by the number of M-cations to which they are bonded. These are the ${}^{[1]}\Phi$- and ${}^{[2]}\Phi$-anions, both of which occur in all possible backbone configurations of chains (*trans*, *lox*, *mik*, and *cis*) and ribbons (Fig. 1a–c), and the ${}^{[3]}\Phi$-anion, which occurs only in *cis*-backbone configurations and ribbons (Fig. 1b–c).

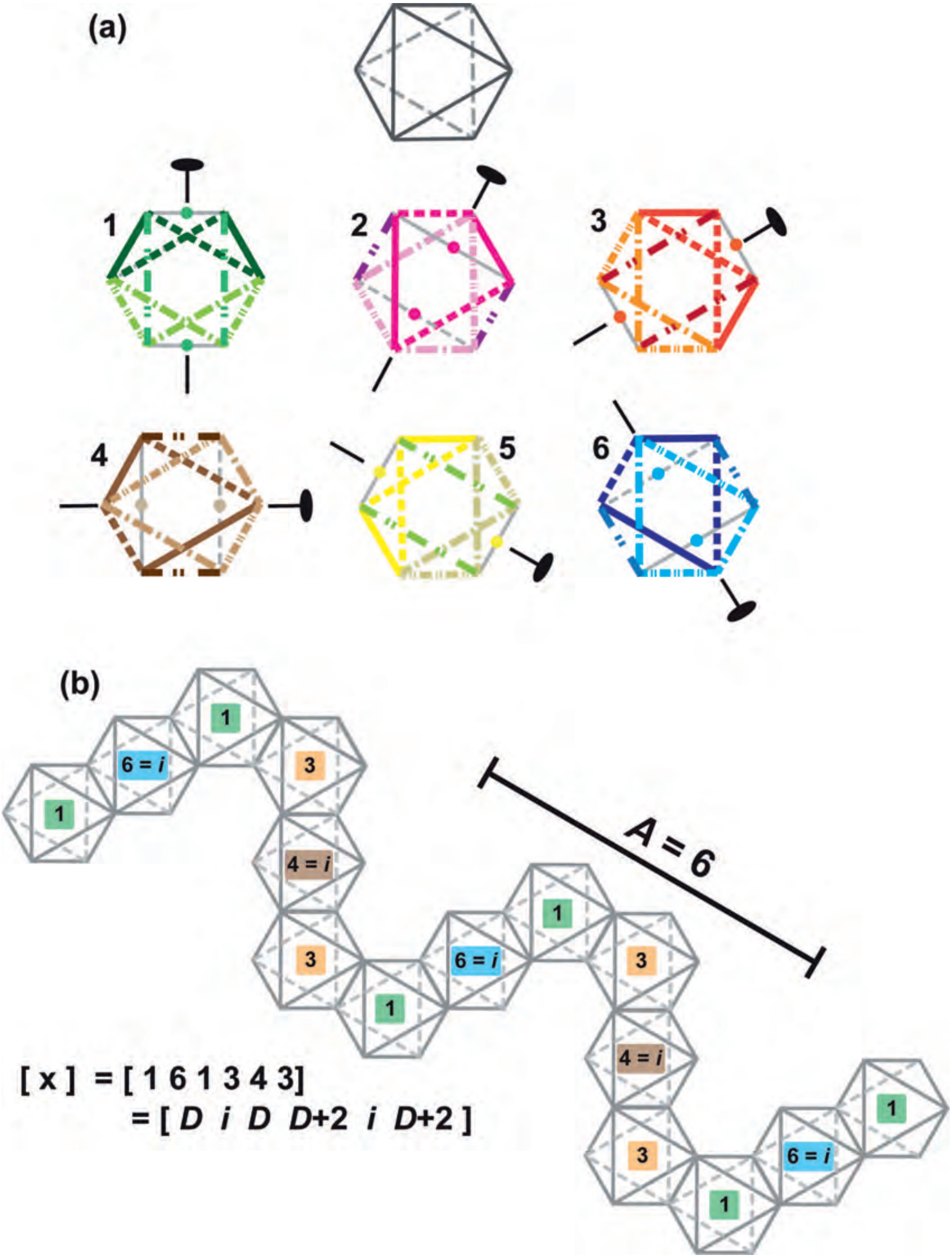

FIG. 2. In non-*cis* backbones, all pairs of shared edges (on a specific octahedron) are relatable by the operation of one of the six octahedral [2]-fold axes or inversions. (a) The orientations of the axes are illustrated, and color-coded, relative to a holosymmetric octahedron. The colored circles indicate the location of entries/exits of the axes on the solid form. Any non-*cis* backbone can be constructed by specifying a sequence of [2]-fold axes operating in successive octahedra. (b) An example of a hypothetical backbone resulting from the sequence [x] = [1 *i* 1 3 *i* 3] = [*D* *i* *D* *D*+2 *i* *D*+2]. Note that the orientation of all octahedra in this figure (as well as Fig. 3b–e) are referenced to the black octahedron in (a).

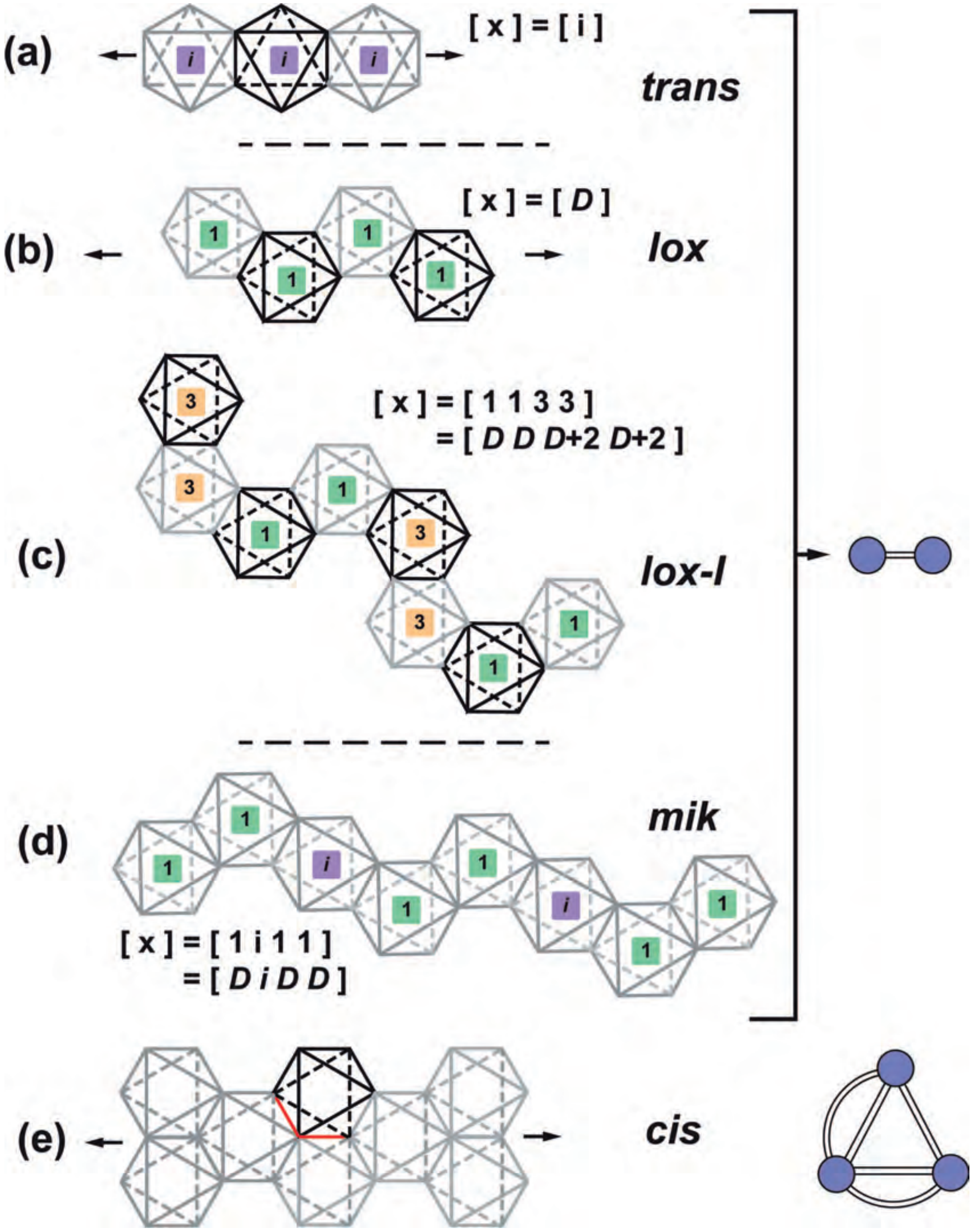

FIG. 3. Backbone topologies commonly observed in minerals. The basic graphical representation, as well the value of [x], defined in the text, is also shown. For simplicity, these are referred to by common names: (a) *trans*, (b–c) *lox*, (d) *mik*, and (e) *cis*. The pair of shared octahedron edges (with a common vertex) as required by the definition of a *cis* chain is highlighted in red.

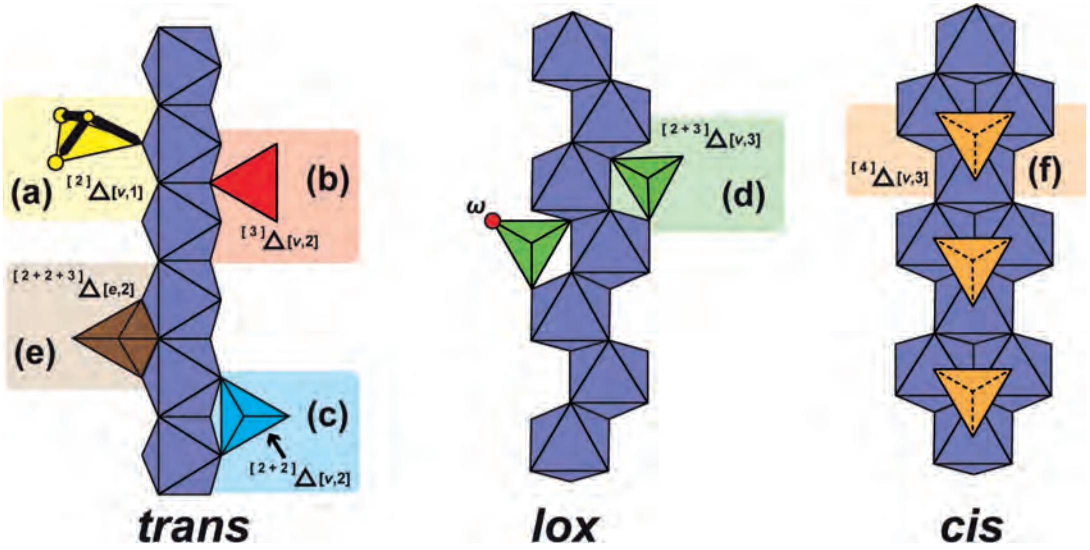

FIG. 4. Decoration polyhedra are distinguished by the coordination state of the anion(s) linking them to backbone octahedra. Six common types are observed in mineral structures: (a) $^{[2]}\Delta[v,1]$-type, (b) $^{[3]}\Delta[v,2]$-type, (c) $^{[2+2]}\Delta[v,2]$-type, (d) $^{[2+3]}\Delta[v,2]$-type, (e) $^{[2+3+2]}\Delta[e,2]$-type, and (f) $^{[4]}\Delta[v,3]$-type.

CONFIGURATION OF DECORATION POLYHEDRA

Decoration polyhedra are characterized by how they are connected to the backbone octahedra as opposed to by chemical species (SiO_4^{4-}, CO_3^{2-}, *etc.*) or by polyhedron geometry (tetrahedron, trigonal planar, *etc.*). Any decoration, $(T\Phi_m)^n$, may be characterized by the coordination numbers of the anions actively linking the backbone and decoration polyhedra. This is denoted by the general term $^{\sum a}\Delta[s,N]$, where Δ indicates a decoration polyhedron, $\sum a$ corresponds to the coordination number of each linking anion, which is written in sequence, *e.g.*, $\sum a =$ [2+2], *s* denotes the shared polyhedral element (*i.e.*, *v* = vertex, *e* = edge, and *f* = face), and *N* corresponds to the number of backbone octahedra with which the decoration is element sharing.

The number of possible values of $^{\sum a}\Delta[s,N]$ is constrained by the geometry of decoration polyhedra and by backbone configuration and is relatively small. An exhaustive approach to determining these illustrated in Figures 4 and 5 shows that there are 21 possible decoration configurations. However, a thorough examination of over 250 chain-bearing structures reveals that only six of these (Fig. 4) are observed in minerals with significant frequency. In general, decorations linked to backbone octahedra by vertex-sharing occur often, whereas those linked to backbone octahedra by edge- and face-sharing occur increasingly less often. The six most commonly observed decoration polyhedra are discussed in greater detail here.

(1) $^{[2]}\Delta[v,1]$-type: Where a decorating polyhedron is linked to the backbone through a common $^{[2]}\Phi$-type anion; thus the anion coordination may be written as *MT* where *M* is a backbone cation and *T* is the cation of a decorating polyhedron (Fig. 4a).

(2) $^{[3]}\Delta[v,2]$-type: Where a decorating polyhedron is linked to the backbone through a common $^{[2]}\Phi$-type anion, resulting in *MMT* coordination of the anion (Fig. 4b).

(3) $^{[2+2]}\Delta[v,2]$-type: Where two vertices of a decorating polyhedron link to two backbone octahedra; each shared vertex corresponds to a $^{[1]}\Phi$-type anion, resulting in *MT* coordination (Fig. 4c).

(4) $^{[2+3]}\Delta[v,3]$-type: Where two vertices of a decorating polyhedron link to three backbone octahedra through a $^{[1]}\Phi$-type anion and a $^{[2]}\Phi$-type anion, resulting in one shared anion with *MT* coordination and the other with *MMT* coordination (Fig. 4d).

(5) $^{[2+3+2]}\Delta[f,2]$-type: Where three vertices of a decorating polyhedron link to two backbone octahedra through sharing of two $^{[1]}\Phi$-type anions and one $^{[2]}\Phi$-type anion, resulting in two anions with *MT* coordination and one with *MMT* coordination; here, two of the decoration edges are also shared (Fig. 4e).

(6) $^{[4]}\Delta[v,3]$-type: Where one vertex of a decorating polyhedron links to three backbone octahedra through a $^{[3]}\Phi$-type anion, resulting in *MMMT*

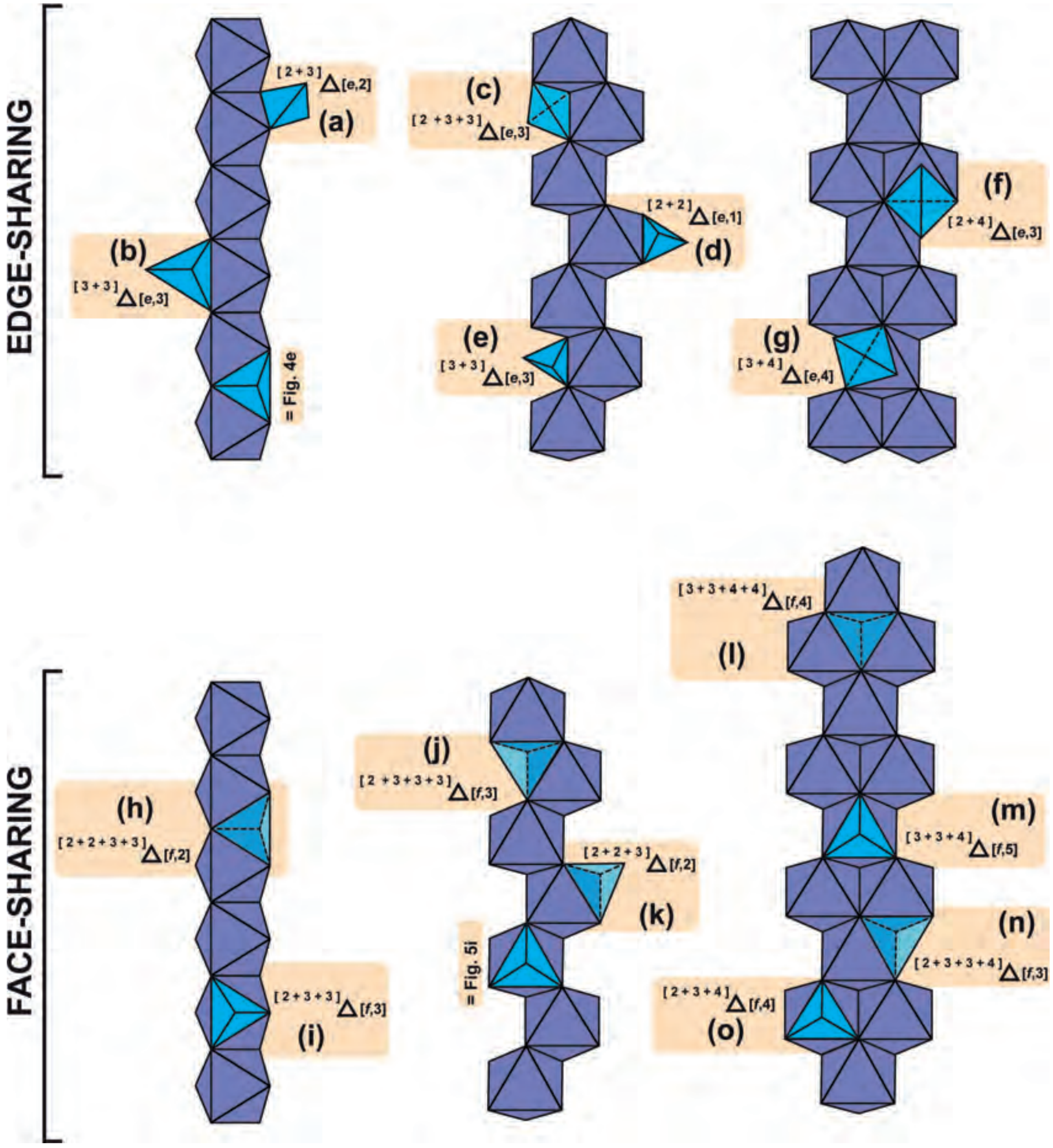

FIG. 5. In addition to those illustrated in Figure 4, 15 additional configurations of [$T\Phi_m$] decoration polyhedra (shown here as tetrahedra, $m = 4$) are possible in *trans*, *lox*, and *cis* chains. Here, these are separated into two groups, those that are related to backbone octahedra by (a–g) edge-sharing and (h–n) face-sharing.

coordination; this decoration type is possible only on *cis*-type chains (see below) and ribbons (Fig. 4f).

Backbone-decoration pairs

The linking of backbone configurations and polyhedral decorations ($^{\Sigma a}\Delta[s,N]$) is limited by the geometric constrains of both, *i.e.*, it is not possible for all values of $^{\Sigma a}\Delta[s,N]$ to link to all backbones. For instance, $^{[3]}\Delta[v,2]$-type decorations can occur on *trans*, *lox*, *mik*, and *cis* chains, whereas $^{[2+2+3]}\Delta[e,2]$-type decorations can occur only on chains with the *trans* backbone. Table 2 lists the 21 possible decoration configurations illustrated in Figures 4 and 5, indicating

TABLE 2. GEOMETRICALLY PERMISSIBLE BACKBONE-DECORATION PAIRS

	$\Sigma^{a}\,\Delta\,[s,N]$	*trans*	*lox*	*cis*	Fig.
(1)	$^{[2]}\,\Delta\,[v,1]$	•	•	•	4a
(2)	$^{[3]}\,\Delta\,[v,2]$	•	•	•	4b
(3)	$^{[2+2+3]}\,\Delta\,[e,2]$	•			4c
(4)	$^{[2+2]}\,\Delta\,[v,2]$	•	•	•	4d
(5)	$^{[2+3]}\,\Delta\,[v,3]$		•	•	4e
(6)	$^{[4]}\,\Delta\,[v,4]$			•	4f
(7)	$^{[2+3]}\,\Delta\,[e,2]$	•	•	•	5a
(8)	$^{[3+3]}\,\Delta\,[e,3]$	•	•	•	5b
(9)	$^{[2+3+3]}\,\Delta\,[e,3]$		•	•	5c
(10)	$^{[2+2]}\,\Delta\,[e,1]$		•	•	5d
(11)	$^{[3+3]}\,\Delta\,[e,3]$		•	•	5e
(12)	$^{[2+4]}\,\Delta\,[e,3]$			•	5f
(13)	$^{[3+4]}\,\Delta\,[e,4]$			•	5g
(14)	$^{[2+2+3+3]}\,\Delta\,[f,2]$	•			5h
(15)	$^{[2+3+3]}\,\Delta\,[f,3]$	•	•		5i
(16)	$^{[2+3+3+3]}\,\Delta\,[f,3]$		•	•	5j
(17)	$^{[2+2+3]}\,\Delta\,[f,2]$		•	•	5k
(18)	$^{[3+3+4+4]}\,\Delta\,[f,4]$			•	5l
(19)	$^{[3+3+4]}\,\Delta\,[f,5]$			•	5m
(20)	$^{[2+3+3+4]}\,\Delta\,[f,3]$			•	5n
(21)	$^{[2+3+4]}\,\Delta\,[f,4]$			•	5o

the chain backbones with which they are geometrically compatible.

Octahedron decorations

Where $3 \leq m \leq 5$, the distinction between decoration and backbone polyhedra is unambiguous: *i.e.*, all octahedra and non-octahedra are included as backbone and decoration, respectively, regardless of attachment conformation. However, adding an octahedron ($m = 6$) to a pre-existing backbone has the possibility of resulting in either a decoration polyhedron or a new backbone (or ribbon) configuration. Distinguishing between these situations is straightforward, and consistent with the above-defined terms: an octahedron is considered part of the backbone if it shares (at least) two edges with (at least) two different octahedra. All other configurations are decorations.

For the chains with backbone configurations illustrated in Figure 3 (*trans*, *lox*, *lox-1*, *cis*), there are four possible configurations with which a non-decoration octahedron can be added to backbones. Consistent with the format of decoration notation, these are denoted as $^{\Sigma a}\Omega[s,N]$: (1) $^{[2+2+3]}\Omega[e,2]$ (*trans* backbone; Fig. 6a); (2) $^{[2+3+3]}\Omega[e,3]$ (*lox* / *cis* backbones; Fig. 6b); (3) $^{[2+2+3+3]}\Omega[e,3]$ (*lox* / *cis* backbones; Fig. 6c–d); and (4) $^{[2+2+3+3+3]}\Omega[e,4]$ (*lox-1* backbone; Fig. 6e). Note: the addition of a $^{[2+2+3+3]}\Omega[e,3]$ octahedron to a *lox* or a *cis* backbone results in the formation of a *cis* backbone (Fig. 6c) and ribbon (Fig. 6d), respectively; the $^{[2+2+3+3+3]}\Omega[e,4]$ octahedron may be added only to a *lox-1* backbone, forming a ribbon (Fid. 6e).

STOICHIOMETRIC FORMULAE FOR DECORATED CHAINS OF EDGE-SHARING OCTAHEDRA

The general stoichiometry of all chains of decorated octahedra may be expressed as follows:

$$^{c}[\,M_{A} \quad T_{X} \quad \Phi_{z}\,] \qquad \text{(Eq. 1)}$$

where the superscript c denotes the backbone configuration, *i.e.*, *trans*, *lox*, *mik*, or *cis*; M is any octahedrally coordinated cation; A is the number of M-cations (or octahedra in a polyhedral representation) in the crystallographic repeat of the chain; and Φ_z is all backbone anions not linked to a decorating polyhedron. For a chain, the complement of decorating polyhedra occur with the stoichiometry

$$(T\Phi_6)_h(T\Phi_5)_i(T\Phi_4)_j(T\Phi_3E)_k(T\Phi_3)_l$$

where

$$X = h + i + j + k + l \qquad \text{(Eq. 2)}$$

For brevity, any chain stoichiometry can be represented as the [1 × 3] matrix

$$^{c}[\,A \quad X \quad z\,] \qquad \text{(Eq. 3)}$$

FINITE GRAPHICAL REPRESENTATIONS OF INFINITE CHAINS

In Graph Theory, a graph is defined as a nonempty set of elements, $V(G)$, called *vertices*, and a nonempty set of unordered pairs of these vertices, E(G), called *edges* (*e.g.*, Wilson 1979). Vertices and labels may be labelled (or colored) to represent objects with specific characteristics. The number of edges incident at a vertex is known as the *degree*, *d*, of the vertex. The structure of any crystal inherently lends itself to graphical representation, with vertices corresponding to elements of the structure (*e.g.*, atoms or polyhedra) and edges corresponding to linkages between those elements. Graphs in which polyhedra are depicted as vertices are very effective ways to represent the topology of complex atomic arrangements (*e.g.*, Hawthorne 1983, 2014, 2015, Hawthorne & Schindler 2000, Burns & Hawthrone 1995, Krivovichev 2008, 2009).

Graphical representations have two major uses in the current context. First, they are effective ways of distilling complex topological information to simple forms that facilitate visual comparison of other

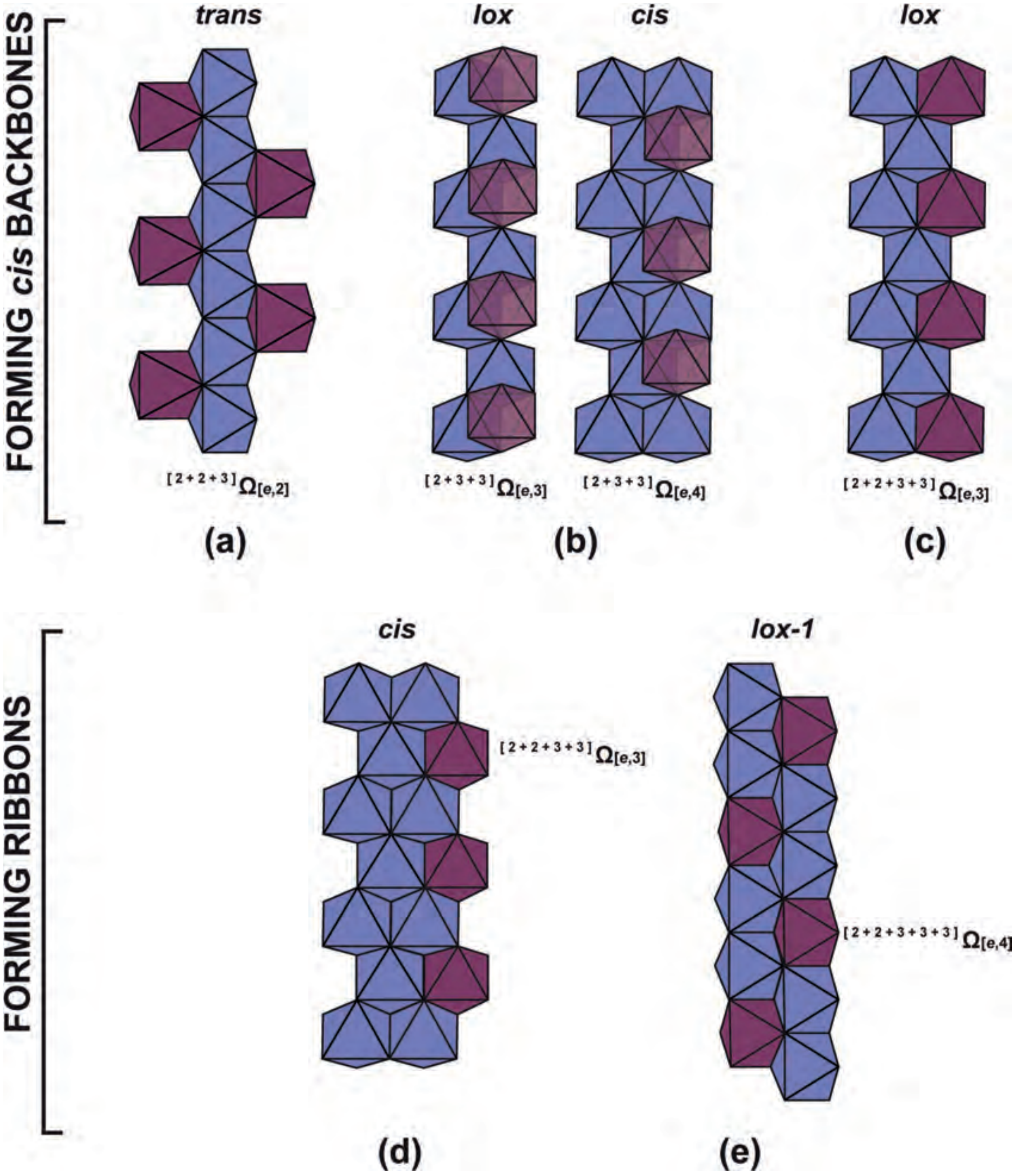

FIG. 6. The addition of backbone octahedra (mauve) to a pre-existing backbone chain (purple), resulting in the formation of (a–c) *cis*-chains, and (d–e) ribbons.

structural entities that have similar (but distinct) topological characteristics. Second, through the application of enumeration methods, it is possible to derive all possible topologies (*e.g.*, Harary & Palmer 1973) for a certain set of conditions. Hawthorne (1983) illustrated the effectiveness of this approach by considering isolated clusters of linked octahedra and tetrahedra. He showed how, by imposing crystal-chemical constraints on graphically possible topologies, a list of potential clusters could be derived. Cross referencing all possible clusters to those that are observed in crystal structures increases our understanding of the crystal-chemical rules governing mineral stability. Both uses are of interest here. The first is directly relevant to the hierarchical classification of chain-bearing structures, which will be developed in subsequent publications. The second is of interest as it provides insight into why, although the number of possible chain-topologies is large, only a relatively small number are observed in minerals.

A graphical representation conveys the topological information regarding the connectivity of chain backbones and decoration polyhedra. Hence, for any given segment of chain considered, there must be a one-to-one correlation between linkages in the polyhedral and graphical representations. However, certain complications arise when trying to represent an infinite object (chain) by a finite graph, thus requiring a more involved discussion.

The coloring of vertices

In the graphs derived here, vertices and edges correspond to polyhedra and linking anions, respectively. The color of vertices distinguishes: (1) backbone vertices from decoration vertices; and (2) the configuration (${}^{\sum a}\Delta[s,N]$) of decoration polyhedra. Vertex coloring in all graphs shown here adheres to the scheme: (1) vertices mapping to backbone octahedra are purple; and (2) vertices mapping to decorations are colored based on values of ${}^{\sum a}\Delta[s,N]$. For the common decoration polyhedra, denoted as ${}^{[4]}\Delta[v,3]$-, ${}^{[2+2+3]}\Delta[v,2]$-, ${}^{[2+3]}\Delta[v,3]$-, ${}^{[2+2]}\Delta[v,2]$-, ${}^{[3]}\Delta[v,2]$-, and ${}^{[2]}\Delta[v,1]$-types, the corresponding vertex colors are orange, brown, green, blue, red, and yellow, respectively. In the text below, the total vertices mapping to all observed decorations, $\sum|{}^{\sum a}\Delta[s,N]|$, in a particular chain may be referred to as decoration (non-purple) vertices. In this scheme, polyhedral geometries are not identified graphically, however, we note that it would be possible to add such information (*e.g.*, by altering the shape of the vertex such as triangle = trigonal planar, square = tetrahedron, *etc.*) without changing any of the significant points discussed.

From infinite chains to finite graphical representations

Consider the derivation of graphical representations for the two chains illustrated in Figure 7. A segment of the undecorated *trans* chain, ${}^{trans}[M\Phi_4]$, is shown in Figure 7a. Such an illustration is referred to as a *segment polyhedron representation,* and the corresponding *segment graph* is derived by a one-to-one mapping of each backbone octahedron to purple (backbone) vertices (Fig. 7b). Similarly, from the segment polyhedron representation of the ${}^{trans}[M_2T_2\Phi_6]$ chain (Fig. 7e), the corresponding segment graph is derived by a one-to-one mapping of backbone octahedra, ${}^{[2]}\Delta[v,1]$-type decoration polyhedra, and ${}^{[3]}\Delta[v,2]$-type decoration polyhedra, to purple, yellow, and red vertices, respectively (Fig. 7f). Vertices are linked by edges corresponding to the sharing of polyhedron vertices.

Although segment graphs are illustrative, they are inherently incomplete and are not useful for graphical enumeration. To overcome this problem, we must derive a graph that: (1) is finite, and (2) correctly represents the connectivity of all vertices (*i.e.*, all vertex degrees must be correct). Because neither chain contains a decoration polyhedra that links to successive crystallographic repeats (see below), deriving the correct graph for the chains in Figure 7 is straightforward; the segment graph is severed at the horizontal dotted lines (*i.e.*, corresponding to the crystallographic repeat; Fig. 7c, g). In order to satisfy the above criteria, the truncated, severed edges are connected, forming looped edges linking purple (backbone) vertices (Fig. 7d, h). The looped edges also indicate how the topology of the complete chain may be generated by translation of a graphical entity.

Crystallographic and topological repeat units

In a chain, the crystallographic and topological repeat units need not be equivalent. For a chain with the general formula ${}^{trans}[\ M_2\ T_2\ \Phi_6]$, a *segment polyhedron representation* (segment length = six backbone octahedra) is illustrated in Figure 8a. In a *geometric segment graph* (Fig. 8b), the relative positions of vertices are drawn to be equivalent to the relative positions of polyhedra in the polyhedron representation. Drawing the graph in such a way is useful, as it promotes an intuitive understanding of the relation between the crystallographic (*i.e.*, translational) and topologic character of a chain.

However, a graph has no geometrical properties, and thus the positions of the vertices may be moved relative to each other without changing the information content of the graph. For instance, moving all red vertices to the same side of the chain results in the graphical representation of Figure 8c. By moving vertices (and preserving edge sets), there are an infinite number of pictorial representations in which the connectivity of the graph is preserved.

Analogous to the crystallographic repeat in the polyhedron representation, the *topologic repeat* is the smallest sub-graph of the segment graph that shows (1) the repeat sequence of backbone (purple) vertices, and (2) all the decorations linked to these backbone vertices. The segment graphs for the ${}^{trans}[M_2T_2\Phi_6]$ chain (Fig. 8b, c) show that all backbone (purple) vertices are topologically equivalent, as are all decoration (red) vertices; each of the former links to

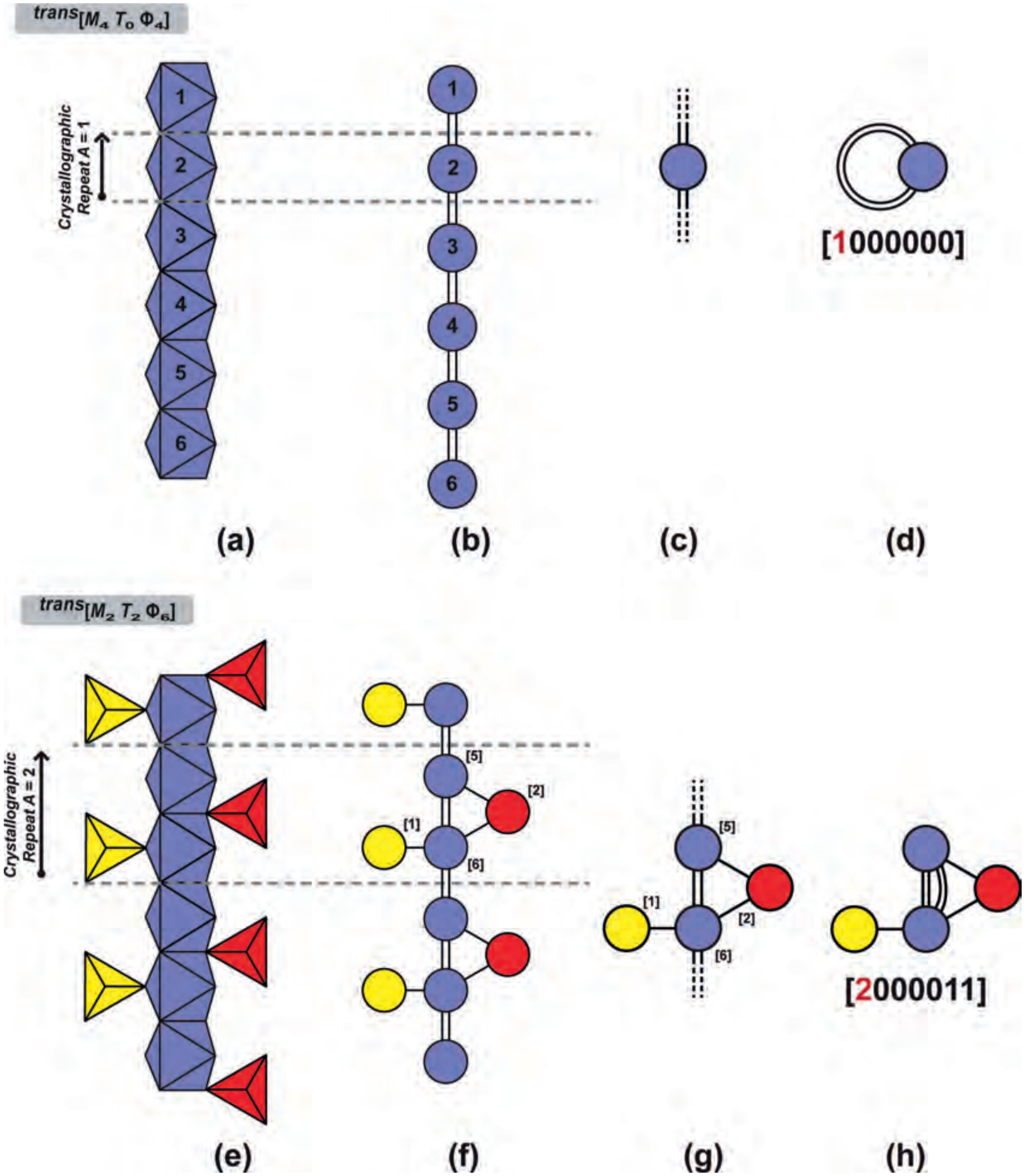

FIG. 7. The derivation of graphical representations. For ${}^{trans}[M_1\ T_0\ \Phi_4]$: polyhedral and graphical representations of a chain segment are illustrated in (a) and (b), respectively. The horizontal dashed lines indicate the crystallographic repeat unit, and the isolated graphical segment is illustrated in (c). In (d) the final finite graph is illustrated, wherein the single vertex is linked to itself with two arched edges. For ${}^{trans}[M_2\ T_2\ \Phi_4]$: analogous polyhedral and graphical representations of a chain segment are illustrated in (e) through (h); color-coding corresponds to decoration nomenclature as outlined in the text.

two decoration and two backbone vertices (degree 6), and each of the latter links to two backbone vertices (degree 2). The topological repeat of the chain contains one topologically unique backbone vertex and the two red vertices linked to it (pink highlighted area in Fig. 8c).

From the topological repeat, we may derive the *irreducible topological repeat graph* of any chain that

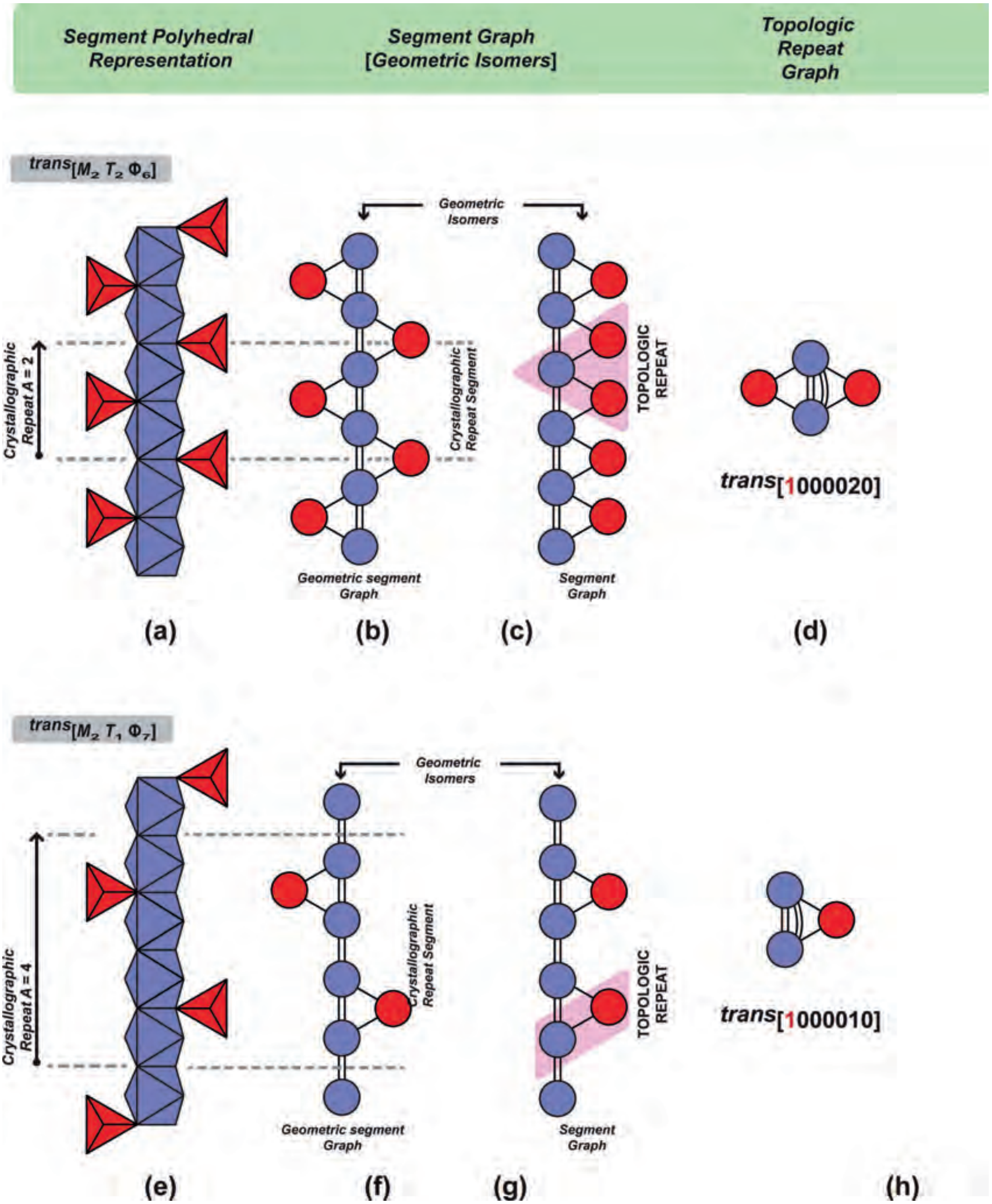

FIG. 8. Crystallographic and topological repeat units need not be equivalent in all chains. For the $^{trans}[M_2\ T_2\ \Phi_5]$ chain: the polyhedral segment (a) has a crystallographic repeat unit equivalent to two octahedra ($A = 2$). Despite being visually different, the two segment graphical representations (b and c) are topologically equivalent and show that each vertex is topologically equivalent. Hence, the finite graphical representation (d) corresponds to ($B = 1$), *i.e.*, ^{trans}[1000020]. The analogous construction is illustrated for the $^{trans}[M_2\ T_1\ \Phi_7]$ chain in (e) through (h). Note: In this and subsequent figures, the B value appears in dark red to distinguish it from other values in the matrix.

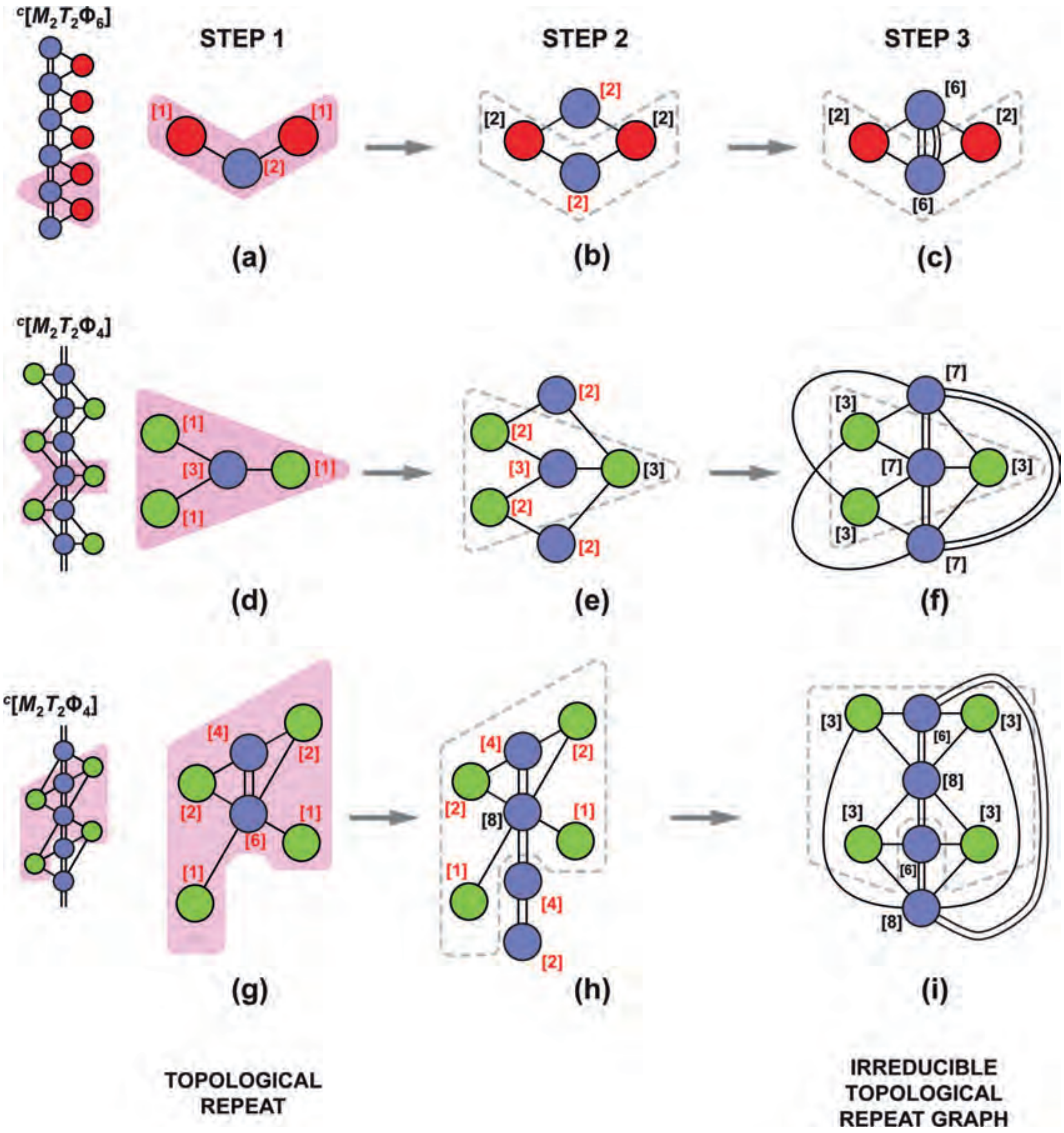

FIG. 9. Stepwise derivation of the irreducible topologic repeat graph from the topologic repeat unit.

satisfies the two graph criteria listed above. This is done by expanding the *topological repeat graph* in a stepwise manner until the degrees of each vertex are correct. The process for doing this is illustrated in Figure 9 for one $^c[M_2T_2\Phi_6]$ chain and two topologically distinct $^c[M_2T_2\Phi_4]$ chains. Correct and incorrect values of degree appear in black and red, respectively.

Step 1: A sub-graph corresponding to the topological repeat unit is drawn (Fig. 9a).

Step 2: The addition of a backbone vertex increases the degrees of the red vertices to the correct value of [2] (Fig. 9b).

Step 3: For the backbone (purple) vertices, linking these to each other increases their degrees to the correct values of [6] (Fig. 9*c*) and results in the topological repeat graph, which, unlike a segment graph, is irreducible. The analogous steps for the $^{trans}[M_2T_2\Phi_4]$ chains are illustrated in Figure 9d–i. In following these steps for any chain, only one topological repeat graph may be derived.

For a chain with decoration polyhedra $\sum|^{\sum a}\Delta [s,N]|$, the number of required backbone (purple) vertices, *B'*, in the irreducible topological repeat graph is either (1) the largest value of *N*, where *N* is an integer multiple of *B* (*i.e.*, *nB*); or (2) the next highest multiple of *nB*, where *N* is not an integer multiple of *B*. For example, the graph corresponding to $^{c}[M_2T_2\Phi_6]$ (Fig. 9a–c) contains two backbone (purple) vertices because max(*N*) = 2, which corresponds to 2*B*; by contrast, the graph corresponding to $^{lox}[M_2T_2\Phi_4]$ (Fig. 9g–h) contains four backbone (purple) vertices as max(*N*) = 3 and *nB* = *n(2)* = [2, 4, 6, …, *nB*].

Topological formulae of chains

The *topological* formula, consisting of a pair of terms, is given by

$$\left([\mathrm{x}],\left[M_B\left({}^{[4]}\mathit{\Delta}[v,3]_o{}^{[2+3+2]}\mathit{\Delta}[e,2]_p{}^{[2+3]}\mathit{\Delta}[v,2]_q{}^{[2+2]}\mathit{\Delta}[v,2]_r{}^{[3]}\mathit{\Delta}[v,2]_s{}^{[2]}\mathit{\Delta}[v,1]_t\right)\right]\right) \qquad \text{(Eq. 4)}$$

The first term, [x], is a matrix indicating backbone configuration; the second term corresponds to the vertex-set of the topological repeat unit (not necessarily the topological repeat graph) and is useful in the hierarchical ordering of chain topologies. As above, *B* is the number of backbone (purple) vertices that occur in the topological repeat unit. The subscripts *o* through *t* denote the total number of each color of non-purple vertex that link to the *B* (purple) vertices. The decoration polyhedra are ordered by decreasing average coordination number of the linking anions. Equation 4 may be condensed to the [1 × 7] matrix

$$([\mathrm{x}],[B \quad o \quad p \quad q \quad r \quad s \quad t]) \qquad \text{(Eq. 5)}$$

In Equations 4–5, only decoration types commonly observed in minerals (*i.e.*, Fig. 4) are included; however, the expansion of these expressions to include any plausible decoration type (*i.e.*, Fig. 5) is straightforward.

The color content of the vertex-set of the irreducible topological repeat graph is

$$V(G) = B' + o + p + q + r + s + t = \sum K_i \qquad \text{(Eq. 6)}$$

where each separate term indicates the number of *K*-colored vertices.

Graphical and geometrical isomerism in chains

The graphical approach to representing chains allows direct comparison of the topology of chains (*i.e.*, irrespective of stoichiometry, chemistry, and decoration-polyhedron geometry). Consider the five (labelled I through V) differently configured *trans* chains in Figure 10, in which polyhedral (Fig. 10a–e), segment geometrical (Fig. 10f–j), and topological repeat graph (Fig. 10k–m) representations are shown. Excepting those illustrated in Figure 10b and 10c, all these chains have different formulae and backbone/decoration connectivities (*i.*e., values of $\sum|^{\sum a}\Delta [s,N]|$). Highlighted regions of the segment graphs show that for each chain, the topological repeat consists of a single, topologically unique backbone (purple) vertex (*i.e.*, $B = 1$) linked to two ($o+p+q+r+s+t = 2$) decoration (non-purple) vertices.

In the finite graphical representations of Figure 10, the decoration (non-purple) vertices are colored grey; this simplification allows a more straightforward comparison of the connectivities between backbone and decoration polyhedra. From the graphical representations, two significant observations can be made. First, the graphs corresponding to chains-II, -III, and -IV are identical (Fig. 10l) – the corresponding chains are *geometrical isomers*, having different arrangements of equivalently connected polyhedra. Second, graphs in Figures 10l and 10m have identical vertex-sets, but different edge-sets – the corresponding chains are *graphical isomers*, having equal numbers of components that are differently connected. Chain-I is not isomeric to the others, despite the similarities noted above.

HIERARCHICAL ORDERING OF CHAIN TOPOLOGIES

In a structure hierarchy, constituent structures are ordered such that topological complexity increases with hierarchical sequence. For hierarchies that consist of minerals with varying dimensionalities of connectivities, this typically takes the following form: isolated polyhedra → cluster → chains → sheet → framework (*e.g.*, silicates, Matchatski 1928, Bragg 1930; sulfates, Hawthorne *et al.* 2000; phosphates, Huminicki & Hawthorne 2002; arsenates, Majzlan *et al.* 2014; tellurates, Christy *et al.* 2016; beryllates, Hawthorne & Huminicki 2002; uranyl oxysalts, Burns 1999, 2005, Lussier *et al.* 2016; borates, Grice *et al.* 1999). Though only chains are considered here, an analogous ordering scheme, where hierarchical order reflects increasing topological complexity, can be developed.

In an ordered series of chains, there should be a general trend toward increasing the connectivity of constituent elements (polyhedra or vertices) with hierarchical depth. As has been shown, multiple attributes (*i.e.*, backbone conformation, number of decorations, connectivity of decorations, crystallo-

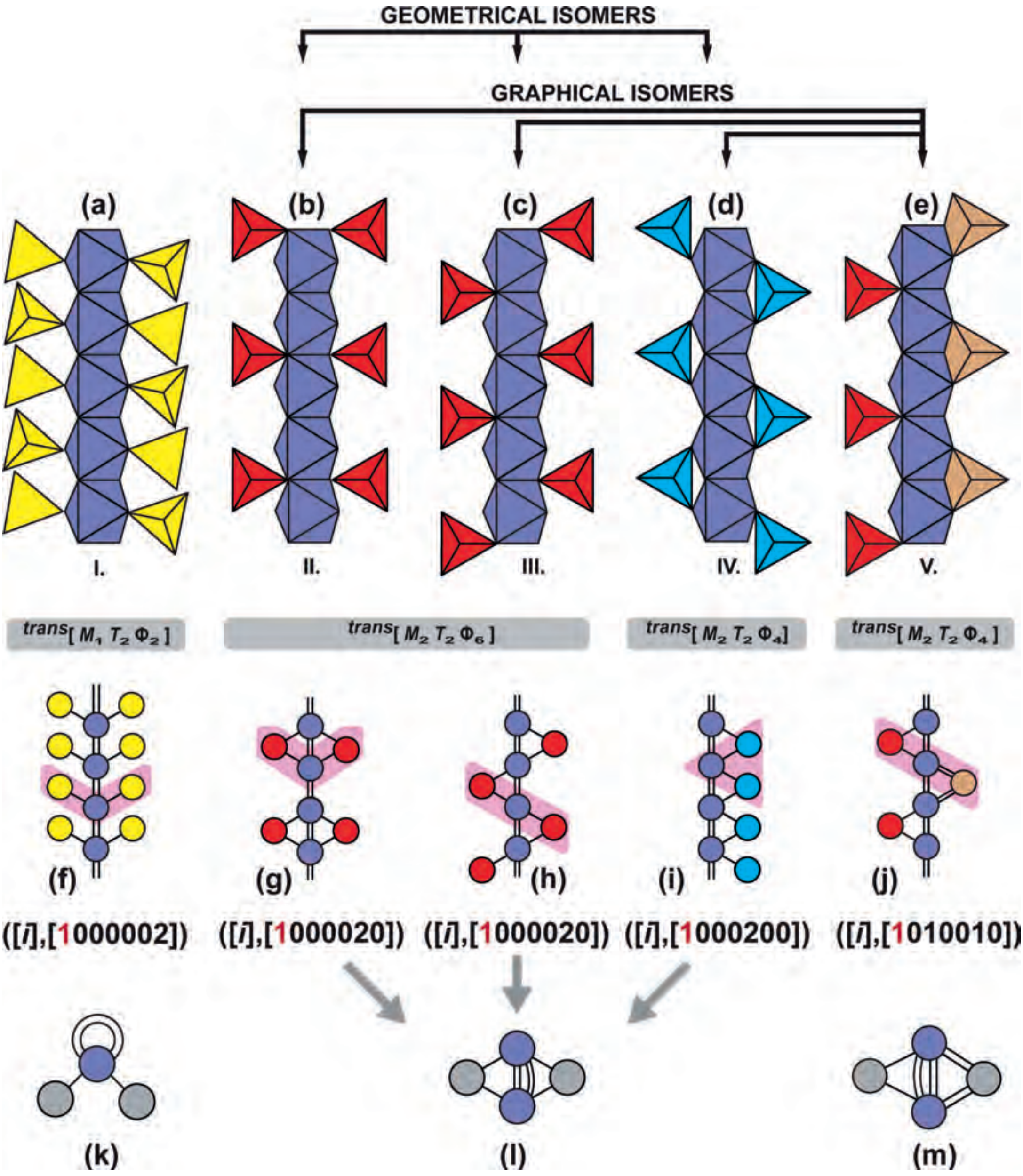

FIG. 10. Graphical *versus* geometrical isomerism in chains of edge-sharing octahedra.

graphic repeat, topological repeat, *etc.*) characterize a chain and any ordering scheme needs to take into consideration multiple pieces of information.

Here, chains are ordered by considering three criteria: (1) the mean connectivity (degree) of backbone (purple) vertices, $<d_{bb}>$; (2) the number of decoration (non-purple) vertices in the topological formula, $\sum_{dec.}(= o + p + q + r + s + t)$; and (3) the mean connectivity (degree) of decorations, $<d_{dec}>$. Chains with unique triplets ($<d_{bb}>$, $\sum_{dec.}$, $<d_{dec}>$) are ordered by the magnitude of $<d_{bb}>$, followed by $\sum_{dec.}$, followed by $<d_{dec}>$. For the following hypothetical series of triplets, order would be: (4,0,0) → (5,1,2) → (5,1,3) → (5,2,1).

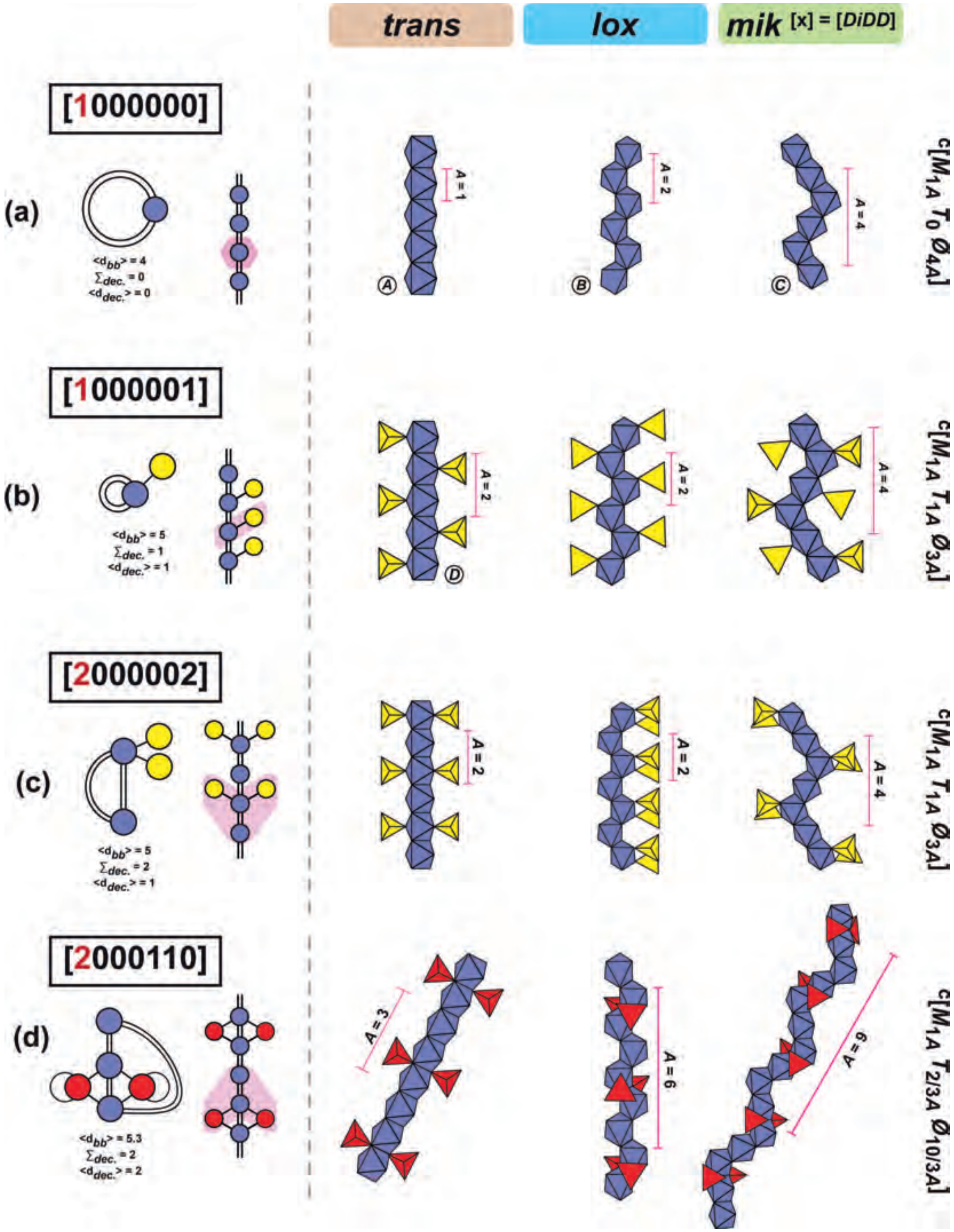

FIG. 11. Examples of observed and hypothetical *trans*, *lox*, and *mik* (where [x] = [1*i*11]) chains ordered hierarchically, based on increasing connectivity of constituent elements. Topological repeats are highlighted in pink. The formulae for non-equivalent backbone configurations are scaled by the crystallographic repeat, *A*. Those occurring in known minerals, as indicated with a circled letter, correspond to: (A) rutile group, $[M^{4+}O_2]$; (B) wodginite group, $[M_4{}^{x+}O_8]$; (C) borax, $\{Na_2(H_2O)_8\}$ $[B_4O_5(OH)_4]$ (Gainsford *et al.* 2008); (D) boralsilite, $[Al_{16}B_6Si_2O_{37}]$ (Peacor *et al.* 1999);

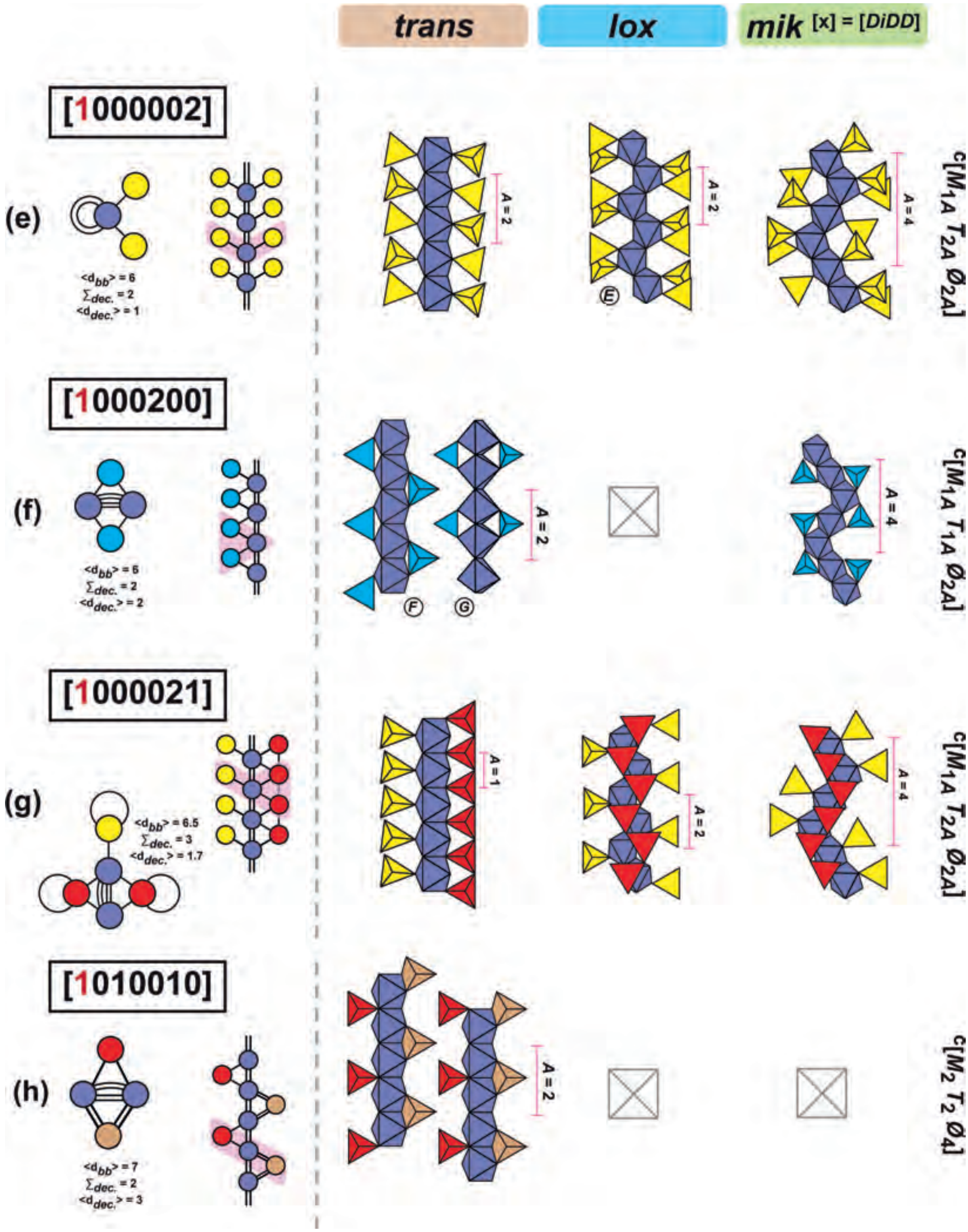

FIG. 11. (continued) (E) stercorite, $\{(NH_4)(H_2O)_4\}$ $[Na(PO_3OH)]$ (Ferraris & Franchini-Angela 1974); (F) linarite, $\{Pb\}$ $[Cu^{2+}(SO_4)(OH)_2]$ (Bachmann & Zemann 1960); (G) mélonjosephite, $\{Ca\}$ $[Fe^{2+}Fe^{3+}(PO_4)(OH)]$ (Kampf & Moore 1977); (H) kentrolite, $\{Pb2\}$ $[Mn_2Si_2O_9]$ (Gabrielson 1962);

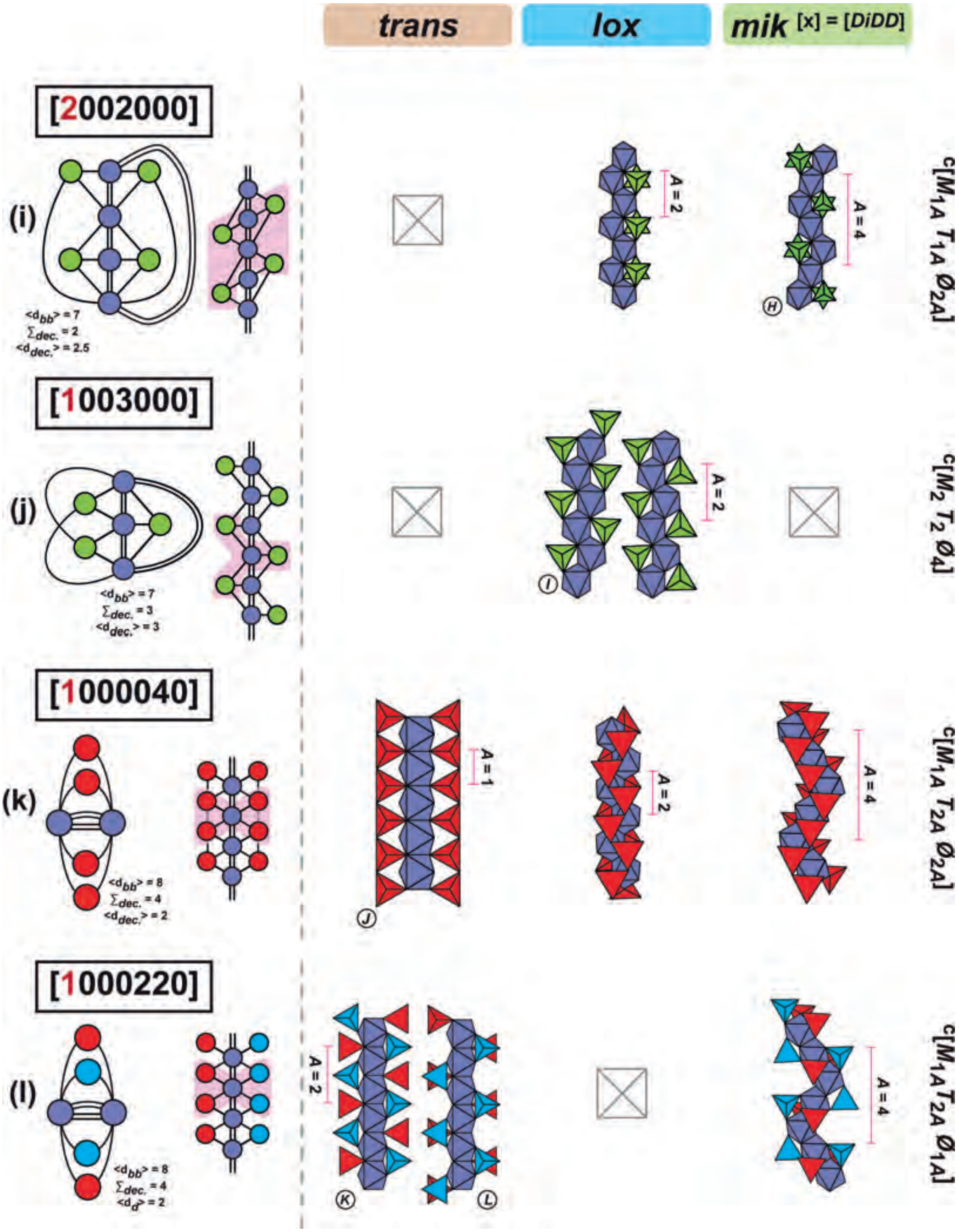

FIG. 11. (continued) (I) yvonite, {H_2O} [$Cu(AsO_3OH)$] (Sarp & Černy 1998); (J) eosphorite, {H_2O} [$MnAl(PO_4)(OH)_2$] (Hoyos *et al*. 1993); (K) falsterite, {$Ca_2(H_2O)_{14}$} [$MgMn^{2+}_2(Fe^{2+}_{0.5}Fe^{3+}_{0.5})_4$ $Zn_4(PO_4)_8(OH)_4$] (Kampf *et al*. 2012); (L) brackebuschite supergroup, {A_2} [$M(TO_4)_2(OH)$]. *Note*: Formulae appear written in binary notation, where { } and [] denote the compositions of the interstitial complex and the structure unit, respectively (see Hawthorne 1985, 1990, 1992).

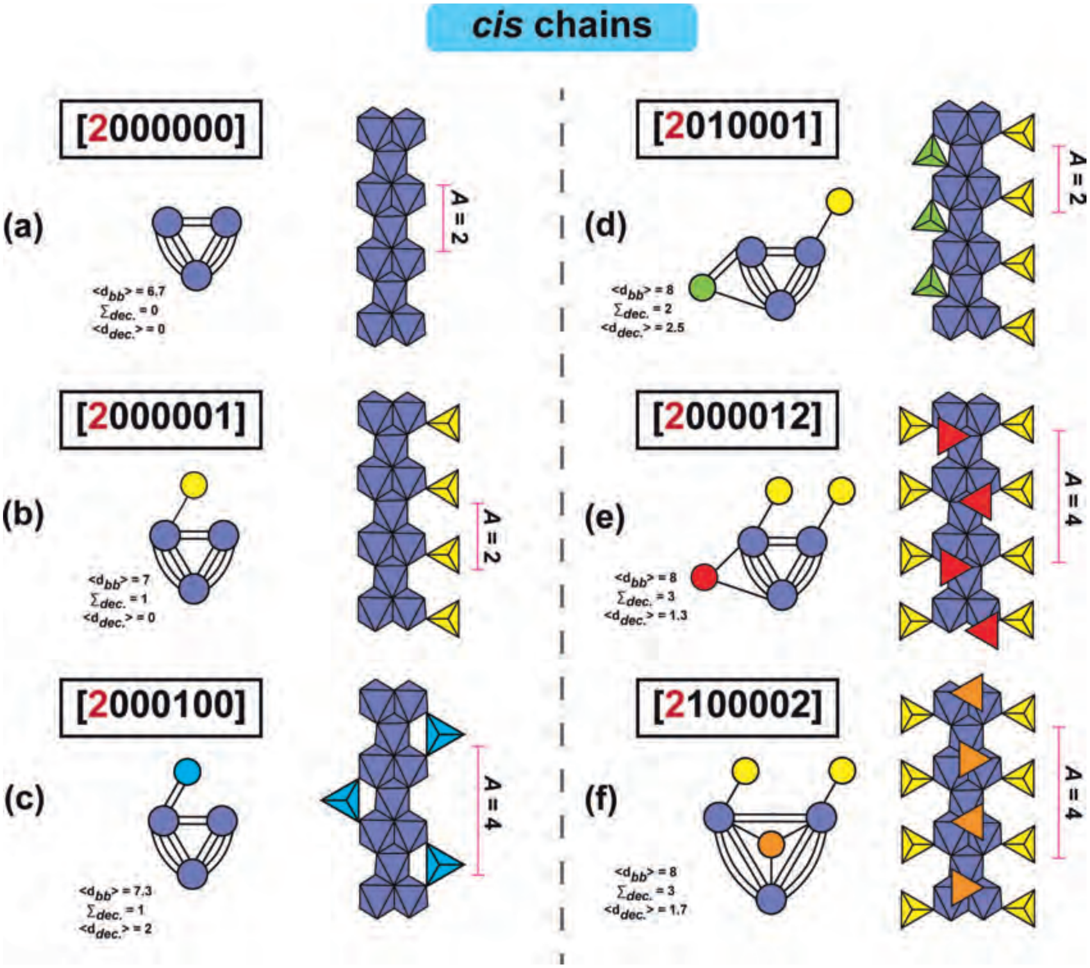

FIG. 12. Examples of *cis* chains ordered hierarchically, based on increasing connectivity of constituent elements.

This is illustrated for a series of chains (both hypothetical and observed) in Figure 11 (*trans*, *lox*, and *mik* backbones) and in Figure 12 (*cis* backbones). This deliberate selection of chains emphasizes many of the concepts (such as graph determination and isomerism) that are introduced above. Important points of note (all referring to Fig. 11) include:

(1) Chains occurring on the same row (regardless of backbone conformation) are of equivalent hierarchical rank (and are geometrical isomers), despite having different crystallographic repeats, *A*. A group of chains formed by rows *k l* are all geometrically isomeric.

(2) A group of chains formed by rows *c*, *f*, and *h* are all graphically isomeric.

(3) The geometric isomers in rows *k* and *l* both have equivalent ($<\mathrm{d_{bb}}>$, $\sum_{\mathrm{dec.}}$, $<\mathrm{d_{dec}}>$) triplets of (8,4,2). In this (relatively) uncommon occurrence, these chains are ordered with increasing mean number of shared vertices linking decorations to the backbone polyhedra. This corresponds to the average number of terms in summations, $\sum$a, for all decorations, $\sum|^{\sum a}\Delta[s,N]|$, in the topological formula. The chains in row *k* show four decorations, each with $^{[2]}\Delta[v,1]$, to the backbone octahedra by sharing one vertex: (1+1+1+1)/4 = 1, whereas the chains in row *l* show two and two decorations linked to backbone octahedra by sharing one ($^{[2]}\Delta[v,1]$) and two ($^{[2+2]}\Delta[v,2]$) vertices, respectively: (1+1+2+2)/4 = 1.5. Hence, chains in row *l* outrank those in row *k*.

SUMMARY

(1) Chains of edge-sharing octahedra are common in minerals. These consist of a backbone of octahedra which may be decorated by other polyhedra.

(2) Four configurations of backbone octahedra are common and are denoted as *trans*, *lox*, *mik*, and *cis*. The sequence of shared edges in octahedra of (non-*cis*) backbones can be defined by the sequence of octahedron [2]-fold rotation operators.

(3) Decoration polyhedra are characterized by the symbol $^{\sum a}\Delta[s,N]$, where the summation $\sum a$ indicates the number and coordination of all linked vertices, and s indicates the dimension of shared elements (v = vertex, e = edge, f = face). There are 21 distinct values of $^{\sum a}\Delta[s,N]$ for chains with *trans*, *lox*, *cis*, and *mik* backbones; however, only 6 of these are common in minerals: $^{[2]}\Delta[v,1]$, $^{[2+2]}\Delta[v,2]$, $^{[3]}\Delta[v,2]$, $^{[2+3]}\Delta[v,2]$, $^{[2+3+2]}\Delta[e,2]$, and $^{[4]}\Delta[v,3]$.

(4) The backbone-decoration connectivity of any chain can be illustrated using either polyhedron or graphical representations.

(5) In the polyhedron representation, the crystallographic repeat is the smallest fragment of a chain that, repeated through translation, shows: (*i*) the configuration of backbone octahedra (*i.e.*, *trans*, *lox*, *cis*, or *mik*), and (*ii*) the stoichiometry, relative positions, and connectivity of the decorating polyhedra.

(6) A chain may be represented graphically with either: (*i*) a segment graph, which is both reducible and infinite in size, and (*ii*) a topologic repeat graph, which is irreducible and has finite size. The topologic repeat unit is the smallest fragment of a segment graph that, repeated through translation, generates the complete segment graph. The topologic repeat is defined by backbone (purple) vertices in the repeating sequence and the number of decoration (non-purple) vertices linked to the topologically unique backbone vertices; it is represented by the matrix [*Bopqrst*].

(7) For any specific chain, there is only one topologic repeat graph; however, multiple chains may correspond to the same topologic repeat graph. Chains corresponding to the same graphs are geometrical isomers.

(8) Chains for which the irreducible graphs have equivalent vertex-sets (where all non-purple vertices are re-cast as monochromatic) but non-equivalent edge sets are graphical isomers.

(9) Using the irreducible graphs, chains may be hierarchically ordered to reflect increasing topological complexity.

ACKNOWLEDGMENTS

The authors are grateful to Anthony R. Kampf and Yulia Uvarova for providing useful comments during the review process. FCH was supported by a Discovery Grant from the Natural Sciences and Engineering Research Council of Canada.

REFERENCES

Bachmann, H.G. & Zemann, J.D. (1960) Kristallstruktur von Linarit, $PbCuSO_4(OH)_2$. *Naturwissenschaften* **47**, 177–177 (in German).

Bragg, W.L. (1930) The structure of silicates. *Zeitschrift für Kristallographie* **74**, 237–305.

Burns, P.C. (1999) The crystal chemistry of uranium. *Reviews in Mineralogy* **38**, 23–90.

Burns, P.C. (2005) U^{6+} minerals and inorganic compounds: Insights into an expanded structural hierarchy of crystal structures. *Canadian Mineralogist* **43**, 1839–1894.

Burns, P.C. & Hawthorne, F.C. (1995) The crystal structure of sinkankasite, a complex heteropolyhedral sheet mineral. *American Mineralogist* **80**, 620–627.

Christy, A., Mills, S., & Kampf, A. (2016) A review of the structural architecture of tellurium oxycompounds. *Mineralogical Magazine* **80**, 415–545.

Ferraris, G. & Franchini-Angela, M. (1974) Hydrogen bonding in the crystalline state: Crystal structure and twinning of $Na(NH_4)(HPO_4)(H_2O)_4$ (Stercorite). *Acta Crystallographica* **B30**, 504–510.

Fleck, M. & Kolitsch, U. (2003) Natural and synthetic compounds with krohnkite-type chains: An update. *Zeitschrift für Kristallographie* **218**, 553–567.

Fleck, M., Kolitsch, U., & Hertweck, B. (2002) Natural and synthetic compounds with krohnkite-type chains: Review and classification. *Zeitschrift für Kristallographie* **217**, 435–443.

Gabrielson, O. (1962) The crystal structures of kentrolite and melanotekite. *Arkiv foer Mineralogi och Geologi* **3**, 141–151.

Gainsford, G.J., Kemmitt, T., & Higham, C. (2008) Redetermination of the borax structure from laboratory X-ray data at 145 K. *Acta Crystallographica* **E64**, 24–25.

Grice, J.D., Burns, P.C., & Hawthorne, F.C. (1999) Borate minerals II. A hierarchy of structures based on the borate fundamental building block. *Canadian Mineralogist* **37**, 731–762.

Harary, F. & Palmer, E. (1973) *Graphical Enumeration*. Academic Press, New York, United States, 271 pp.

Hawthorne, F.C. (1983) Graphical enumeration of polyhedral clusters. *Acta Crystallographica* **A39**, 724–736.

Hawthorne, F.C. (1985) Towards a structural classification of minerals – the $^{VI}M^{IV}T_2\Phi_N$ minerals. *American Mineralogist* **70**, 455–473.

Hawthorne, F.C. (1986) Structural hierarchy in $^{VI}M_X{}^{III}T_Y\ \Phi_Z$ minerals. *Canadian Mineralogist* **24**, 625–642.

Hawthorne, F.C. (1990) Structural hierarchy in $M_6T_4\Phi_N$ minerals. *Zeitschrift für Kristallographie* **192**, 1–52.

Hawthorne, F.C. (1992) The role of OH and H_2O in oxide and oxysalt minerals. *Zeitschrift für Kristallographie* **201**, 183–206.

Hawthorne, F.C. (1998) Structure and chemistry of phosphate minerals. *Mineralogical Magazine* **62**, 141–164.

Hawthorne, F.C. (2014) The structure hierarchy hypothesis. *Mineralogical Magazine* **78**, 957–1027.

Hawthorne, F.C. (2015) Toward theoretical mineralogy: A bond-topological approach. *American Mineralogist* **100**, 696–713.

Hawthorne, F.C. & Huminicki, D.M.C. (2002) The crystal chemistry of beryllium. *Reviews in Mineralogy and Geochemistry* **50**, 333–403.

Hawthorne, F.C. & Schindler, M. (2000) Topological enumeration of decorated $[Cu^{2+}\Phi_2]_N$ sheets in hydroxy-hydrated copper-oxysalt minerals. *Canadian Mineralogist* **38**, 751–761.

Hawthorne, F.C., Krivovichev, S.V., & Burns, P.C. (2000) The crystal chemistry of sulfate minerals. *In* Sulfate Minerals – Crystallography, Geochemistry, and Environmental Significance. *Reviews in Mineralogy and Geochemistry* **40**, 1–112.

Hoyos, M.A., Calderon, T., Vergara, I., & Garcia-Sole, J. (1993) New structural and spectroscopic data for eosphorite. *Mineralogical Magazine* **57**, 329–336.

Huminicki, D.M.C. & Hawthorne, F.C. (2002) Hydrogen bonding in the crystal structure of seamanite. *Canadian Mineralogist* **40**, 923–928.

Kampf, A.R. & Moore, P.B. (1977) Melonjosephite, calcium iron hydroxy phosphate: Its crystal structure. *American Mineralogist* **62**, 60–66.

Kampf, A.R., Mills, S.J., Simmons, W.B., Nizamoff, J.W., & Whitmore, R.W. (2012) Falsterite, $Ca_2Mg\ Mn^{2+}_2\ Fe^{2+}_{0.5}Fe^{3+}_{0.5})_4Zn_4(PO_4)_8(OH)_4(H_2O)_{14}$, a new secondary phosphate mineral from the Palermo No. 1 pegmatite, North Groton, New Hampshire. *American Mineralogist* **97**, 496–502.

Kolitsch, U. & Fleck, M. (2005) Second update on compounds with krohnkite-type chains. *Zeitschrift für Kristallographie* **220**, 31–41.

Krivovichev, S.V. (2008) *Structural Crystallography of Inorganic Oxysalts* **22**. International Union of Crystallography Monographs, Oxford University Press, Oxford, England.

Krivovichev, S.V. (2009) *Structural Mineralogy and Inorganic Crystal Chemistry*. St. Petersburg University Press, St. Petersburg, Russia, 398 pp.

Lussier, A.L., Lopez, R.A.K., & Burns, P.C. (2016) A revised and expanded structure hierarchy of natural and synthetic hexavalent uranium compounds. *Canadian Mineralogist* **54**, 177–283.

Majzlan, J., Drahota, P., & Filippi, M. (2014) Paragenesis and crystal chemistry of arsenic minerals. *Reviews in Mineralogy and Geochemistry* **79**, 17–184.

Matchatski, F. (1928) Zur Frage der Struktur und Konstitution der Feldspate. *Zentralblatt für Mineralogie Abhandlungen A* **1928**, 97–104.

Moore, P.B. (1970) Crystal chemistry of the basic iron phosphates. *American Mineralogist* **55**, 135–169.

Moore, P.B. & Araki, T. (1974) Roweite, $Ca_2Mn^{2+}_2(OH)_4B_4O_7(OH)_2$: Its atomic arrangement. *American Mineralogist* **59**, 60–65.

Moore, P.B. & Araki, T. (1977) Overite, segelerite, and jahnsite; a study in combinatorial polymorphism. *American Mineralogist* **62**, 692–702.

Peacor, D.R., Rouse, R.C., & Grew, E.S. (1999) Crystal structure of boralsilite and its relation to a family of boroaluminosilicates, sillimanite, and andalusite *American Mineralogist* **84**, 1152–1161.

Sarp, H. & Černy, R. (1998) Description and crystal structure of yvonite, $Cu\ (AsO_3OH)\cdot 2(H_2O)$. *American Mineralogist* **83**, 383–389.

Sokolova, E.V. & Hawthorne, F.C. (2004) The crystal chemistry of silicate minerals with chains of (TiO_6) octahedra. *Canadian Mineralogist* **42**, 807–824.

Wilson, R.J. (1979) *Introduction to Graph Theory*. 4th Edition, Longmans, London, England, 184 pp.

Received May 29, 2020. Revised manuscript accepted August 17, 2020.